SAND79-0115
Unlimited Release

INTERIM SUMMARY OF SANDIA CREEP EXPERIMENTS ON ROCK SALT FROM THE WIPP STUDY AREA, SOUTHEASTERN NEW MEXICO

MASTER

W. R. Wawersik and D. W. Hannum

Sandia Laboratories

SF 2900 Q(7-73)

CONTENTS

TABLES AND FIGURES

INTRODUCTION

This report presents an interim summary of triaxial creep experiments which have been performed at Sandia Laboratories on rock salt from the WIPP study area near Carlsbad, New Mexico. The data presented support ongoing efforts to formulate suitable constitutive equations to predict the response of rock salt from southeastern New Mexico to the perturbations of a radioactive waste repository.

The creep experiments of this account are part of an initial test matrix which was defined by Sandia Laboratories and which is being filled by Sandia Laboratories and by RE/SPEC, Inc. This matrix was established to measure the time-dependent behavior of New Mexico rock salt as a function of principal stress difference (deviator stress), confining pressure or mean stress and temperature. The importance of these parameters was suggested by some published data for rock salt and potash (1-8) under low confining pressure $\sigma_2 = \sigma_3 \leq$ 3000 psi (20.7 MPa) which is likely to be typical for the proposed Waste Isolation Pilot Plant. The relevance of all four parameters was further indicated by site specific results of short term (quasi-static) tests which preceded or accompanied creep experimentation in an earlier phase of the Sandia program (9-12).

The creep experiments which will be described here include 23 tests subjected to principal stress differences between 930 psi (6.4 MPa) and 4800 psi (33.1 MPa) and confining pressures between zero (unconfined) and 3000 psi (20.7 MPa). The test temperatures were 22, 100 and 200°C.

The present results, combined with earlier data of RE/SPEC, Inc., indicate further study is required to completely describe the response of New Mexico rock salt under general, time-varying conditions of stress and temperature. To achieve this goal, tests of longer duration are needed, including creep rupture experiments. Furthermore, extension tests and possibly, straight-pull tension tests are adviseable. Finally, additional experiments should be performed to treat data scatter statistically, to account for the unknown effects of impurities and grain size of New Mexico rock salt and to consider differences in salt core histories.

SUMMARY OF BASELINE (QUASI-STATIC) EXPERIMENTS

The nature and sequence of creep experiments completed to date are influenced directly by observations which were made in short-term, so-called quasi-static experiments (12). The majority of these tests were carried out on salt core from drill holes AEC #7 and ERDA #9 at a mean low loading rate 30 (0.21) $\leq d(\sigma_1 - \sigma_3)/dt \leq$ 60 (0.41 MPa/min) psi/min. This loading rate was chosen primarily to compare the results for New Mexico rock salt with extensive published data for rock salt (for example 6). Supplementary experiments were also performed at loading rates up to approximately 20,000 psi/min (0.14 GPa/min).

The following results are deemed particularly pertinent (12).

(1) New Mexico rock salt in the laboratory is very non-linear under all loading conditions with an initial elastic limit $(\sigma_1 - \sigma_3) \approx 0$. This behavior appeared to be unaffected by differences in hydrostatic pressure history to 5000 psi (34.5 MPa) prior to deviatoric loading. It is conceivable that the low initial elastic limit is influenced by damage during coring in situ and subsequent core handling. However, it is impossible at present to separate out this effect because the exact stress history of the material before laboratory testing remains unknown.

(2) The elastic properties of New Mexico rock salt can be evaluated accurately only in load/unload/reload cycles provided the imposed loading rate is sufficiently high or the range of stresses, either hydrostatic pressure p or $(\sigma_1 - \sigma_3)$, is well below the previously attained peak stress. If the elastic constants are evaluated in this manner, then Young's modulus, E, and Poisson's ratio, ν, fall into the ranges $4.3 \times 10^6 \leq E \leq 5.3 \times 10^6$ psi $(29.6 \leq E \leq 36.5$ GPa) and $0.17 \leq \nu \leq 0.26$. These data compare very favorably with in situ measurements based on records of p- and s-wave velocities and rock densities (13).

(3) [illegible]-static [illegible] recovery measurements indicate that [illegible] all nonelastic rock salt deformation is permanent. Addition[illegible], the elastic deformation of New Mexico rock salt subject to deviatoric loading [illegible] a very small fraction of the total deformation.

(4) So far it has been impossible to separate the permanent deformation of rock salt into time-independent and time-dependent components even at the [illegible] high loading rate, $d(\sigma_1 - \sigma_3)/dt$ = 20,000 psi/min ([illegible] GPa/min).

(5) At low confining pressures $\sigma_2 = \sigma_3 \leq 3000$ psi (20.7 MPa) New Mexico rock salt exhibits regimes in which deformation approaches isovolumetric conditions and in which deformation is associated with large dilatancy due to [illegible] fracturing. It appears that the [illegible] isovolumetric, ductile behavior predominates at low deviatoric stress, $(\sigma_1 - \sigma_3) \leq 1100$ psi (7.[illegible] MPa) [illegible], at elevated confining pressure, $\sigma_2 = \sigma_3$ = [illegible] psi ([illegible] MPa) and/or at elevated temperatures [illegible].

(6) Strength and/or ductility of New Mexico rock salt depend on temperature and pressure. According to Table 1, at ambient temperature the ultimate (true) stresses and the corresponding greatest compressive strains, ϵ_1, vary from approximately [illegible] psi ([illegible] MPa) and 2% in uniaxial compression to [illegible] psi ([illegible] MPa) and [illegible] $\leq \epsilon_1 \leq$ 14% at 500 psi (3.5 MPa) confining pressure. At [illegible] psi ([illegible] MPa) confining pressure no signs of macroscopic failure were observed below [illegible] psi ([illegible] MPa) and ϵ_1 = 20%. Macroscopic failure was associated with large principal strain ratios ϵ_3/ϵ_1. For example, when the ultimate stress was reached the ratio ϵ_3/ϵ_1 amounted to -1.[illegible], and -0.[illegible] at zero and 500 psi (3.5 MPa) confining pressure, respectively. By comparison at 3000 psi (20.7 MPa) confining pressure, the greatest observed principal strain ratio was ϵ_3/ϵ_1 = -0.69. Temperature produced a

TABLE [illegible].

[illegible] Stress and Strain (Ductility) Data of Short-Term Loading Tests ([illegible] psi/min [illegible] MPa/min)
Stress and strain represent true stress and engineering strain, respectively.

Test Code (Hole# - Depth (ft)/ conf. press. (ksi)/Temp. °C)	Ultimate (Max) Princ. Stress Diff. (psi)	Ultimate (Max) Princ. Stress Diff. (MPa)	Strain ε1 at Ultimate Stress (%)
	Upper Level Salt		
9-2033/0/23	24[illegible]	16.[illegible]	1.6
9-2080.5/.5/23	[illegible]100	42.1	10.5
9-2[illegible]1.5/3./23	>6000*	>42.1	>20
	Lower Level Salt		
9-2[illegible]6/0/23	330[illegible]	[illegible]	[illegible]
9-2675.[illegible]/0/23	33[illegible]	2[illegible].1	2.4
[illegible]-2[illegible]89/.1/2[illegible]	[illegible]	[illegible]	[illegible].6
7-2[illegible]37/.25/[illegible]	[illegible]3[illegible]	[illegible]	[illegible]
[illegible]-272[illegible]/.5/[illegible]	[illegible]	[illegible]	[illegible]
[illegible]-2[illegible]61/.5/[illegible]	[illegible]*	[illegible].1	[illegible]
[illegible]-2[illegible]1.[illegible]/[illegible]	>[illegible]*	[illegible]	>[illegible].1
[illegible]-26[illegible]/.5/1[illegible]	≈[illegible]30[illegible]	2[illegible].6	≈21
7-2836/[illegible]/20[illegible]	≈210[illegible]	14.5	≈[illegible]
[illegible]-260[illegible]/.5/200	≈[illegible]	[illegible]	≥1[illegible]
[illegible]	≈[illegible]	[illegible]	≥[illegible]

*[illegible]

[illegible] Experiment [illegible] terminated [illegible] [illegible] strains prior [illegible] reaching the ultimate stress.

pronounced decrease in ultimate stress and extended the rock salt ductility, i.e. the amount of rock salt deformation prior to a loss in load bearing ability (Table 1).

(7) Fracture at ambient temperature appears brittle and is followed by a near vertical post-failure curve up to approximately 250 psi (1.7 MPa) confining pressure. The slope of the post-failure curve in stress-strain space increases, i.e. becomes less negative, around and above 500 psi (3.5 MPa) confining pressure. At 200°C unconfined "failure" developed at $(\sigma_1 - \sigma_3) = 2100$ psi (14.5 MPa) and $\epsilon_1 \approx 12\%$.

The foregoing summary of quasi-static experimental results is based primarily on approximately fifty triaxial experiments which were performed on 3.9 in (10 cm) diameter core specimens at Sandia Laboratories. It is supported by additional uniaxial experiments on 4.25 in (10.8 cm) diameter samples and on 2 in (5.1 cm) diameter samples by RE/SPEC, Inc.(9). Though most of these short-term data were remarkably reproducible both qualitatively and quantitatively, it must be recognized that only the unconfined data of RE/SPEC, Inc.(9) might be significant statistically. Shortage of like core made it impossible to repeat experiments in large numbers at all stresses and temperatures of interest. Furthermore the interpretation of experimental results remains incomplete unless mineralogical and textural variation of core are accounted for.

CREEP EXPERIMENTS

Apparatus and Experimental Procedures

All creep experiments were performed in new triaxial apparatus which accommodate relatively large cylindrical samples of up to 4.25 in (10.8 cm) diameter and 8.5 in (21.6 cm) in length. A schematic of this equipment is included as Fig. 1. Axial holes through the top of the pressure vessel and through the loading piston (Part 4) make it possible to vent the specimens by means of appropriate end-caps. Fig. 1 also indicates the use of multiple heaters to compensate for conduction heat losses through the floating base of the pressure vessel.

Testing is accomplished according to the following procedures. Each specimen is coated with a thin layer of RTV Silastic 108 (or equivalent), placed between two steel end-caps and enclosed in a Viton Jacket. The specimen dimensions vary between 3.38 and 3.95 in (9.86 - 10.00 cm) in diameter by 8.00 to 8.30 in (20.3 - 21.1 cm) in length. In turn, the diameter of the end-caps is either 4.1 in or 4.3 in (10.4 - 10.9 cm) depending on the final sample diameter which is anticipated in any particular experiment.

To ensure good alignment all specimen ends are machined parallel to ±0.001 in (±0.03 mm). End effects at the interface between rock salt and end-caps are minimized by polishing the end-cap faces to a mirror finish. Also, thin layers of molybdenum disulfide (Molykote) are provided between sample and end-caps.

Restraints which are generated by the Viton Jackets are small. For a typical wall thickness, t ≈ 0.06 in (1.5 mm), and for the standard internal jacket diameter, D = 4.0 in (10.2 cm), 5 psi (34 kPa) of internal air pressure produce diameter changes of 128% at the midlength of the jacket and 27% at the rock/end-cap interface approximately 1 in (2.5cm) away from a stiff clamp.

After jacketing, each specimen is placed inside the pressure vessel, pressurized hydrostatically and heated if desired, in that order. Heating is accomplished in 50°C increments over periods of two hours per temperature increment. After the target temperature is reached an additional soak period of no less than four hours is added. Overall, regardless of temperature, at least twelve hours elapse between the time of hydrostatic pressurization and the time at which a constant deviatoric stress is superimposed to initiate creep.

Deviatoric loading is achieved rapidly by opening a hand valve between the main loading ram (Part 2) in Fig. 1 and sets of 5 gal (0.02 m^3) precharged accumulators. The exact rate of deviatoric loading is determined in part by the magnitude of the final ram load (principal stress difference) and by the specimen compliance which depends on temperature. However, the loading rate is dictated primarily by the flow resistance of 1/4 in I.D. (6.4 mm) line tubing. Typically, the deviatoric loading rate falls into the range 3500 to 7000 psi/min (24.1 - 48.2 MPa/min).

Once a creep test is underway the ram load is maintained constant unless measurements of specimen area call for manual updates so as to maintain an approximately fixed value of principal stress difference. In turn, confining pressure is regulated intermittently by means of a servo-controlled pressure regulator (14).

In practice the number of system updates and therefore, the accuracy in the control of both $(\sigma_1 - \sigma_3)$ and σ_3 varies depending on the observed creep rates. It also depends sensitively on ambient temperature variations which influence the feed-back signal of the confining pressure system. In view of all these parameters, the range of optimum to worst control lies between [illegible] MPa) and [illegible] psi ([illegible] MPa) for principal stress differences and between [illegible] MPa) and [illegible] psi ([illegible] MPa) in confining pressure [illegible] [illegible] specimen. Considerably higher accuracies can be [illegible] in [illegible] experiments lasting [illegible] from [illegible] hours.

[illegible] completion of any experiment where creep was sustained [illegible] successive stages of decreasing and/or increasing stress differences, the specimen is unloaded to a state of hydrostatic compression. At that point in some cases attempts are made to record specimen recovery. Alternatively, [illegible] specimen recovery are monitored beginning approximately [illegible] after the sample has been removed from the pressure vessel.

[illegible], at the end of each test at elevated temperature, the specimens were [illegible] hours inside the pressure vessel but at [illegible]. In later experiments, sample cooling procedures [illegible]

Instrumentation, Measurements and Data Acquisition

[illegible] force (principal stress difference) and confining pressure are measured outside of the pressure vessel. O-ring friction effects are negligible. [illegible] part standard strain gauge instrumented transducers are employed [illegible] by water cooled copper jackets. Standard Heise gauges with [illegible] are used as backups to measure ram pressure and confining pressure in the event of transducer malfunctions and/or electrical power failures.

Specimen temperature is given directly by the output of the control thermocouples of the two heaters which are shown in Fig. 1. This procedure proved accurate to within ±0.8°C after calibrations established an [illegible] between the temperatures at the thermocouple locations and the temperature over the entire length of the test piece.

To determine axial and radial strain (shear and volume deformation), the total axial sample shortening and the average radial "bulging" of each specimen are measured. The former is accomplished by means of an externally mounted linear variable differential transformer (LVDT). The latter measurement is made by tracking the volume (dilatometric) adjustments of the confining pressure fluid which are necessary to hold the confining pressure fixed ([illegible]). Details concerning all deformation measurements and a number of calibrations are described elsewhere ([illegible]). However, it is reiterated here that records of fluid volume changes are distorted by drift (± 0.8°C in the ambient laboratory temperature. Although such drift usually is diurnal in nature and, therefore, identifiable in long-term creep tests, it can result in errors of as much as ± 0.04% radial strain. Errors of this magnitude can become overriding at low creep rates, less than approximately $5 \times 10^{-9}\ s^{-1}$.

Data acquisition is accomplished by means of a multichannel, partially programmable electronic data logger (Esterline Angus, model PD2064) and a data terminal with casette tape system (Texas Instruments Silent 700, ASR series with 733 tape unit). Five parameters are monitored at intervals of one hour or less: time, ram load (Fig. 1), confining pressure, LVDT signal and dilatometer output. All raw data are transferred at appropriate times onto a PDP 11/34 laboratory computer for reduction and display on a Tektronix 4010 graphics terminal.

MATERIAL DESCRIPTION

Detailed descriptions of New Mexico rock salt from drillholes [illegible] and [illegible] were given in two references (16, 17). The core used here was primarily from drillhole ERDA #9, depth 2050 – [illegible] ft (641 – [illegible] m) and [illegible] – [illegible] ft ([illegible] – 841 m). Typically the rock salt was medium to coarse grained ([illegible] – 1[illegible] mm and 1[illegible] – 20 mm). Larger grains were encountered locally but have been avoided so far in this study. The grain size of all accessory minerals varies from very fine-grained (< 0.1 mm) to fine grained (0.1 – 1 mm). The average water content of rock salt core over the depths of interest was [illegible] (17).

Microscopic examinations (16) indicated that the upper level salt consisted of [illegible] – [illegible] modal per cent halite. Accessory minerals and their ranges were given as: polyhalite 1 – 6%, anhydrite tr–[illegible]% (tr indicates traces), and clay and silt nondiscernable–2%. The lower level salt, ERDA #9, [illegible] – [illegible] ft ([illegible] – 841 m) and AEC #7, 2777 ft ([illegible] m) contained at least 94 modal per cent halite. Polyhalite amounted to tr–5%, anhydrite from tr–3%.

The foregoing microscopic description is in poor agreement with qualitative, mesoscopic observations (16) which indicate high percentages of clay (up to 20%) in core from ERDA #9, 2075 – 2091 ft (640 – 652 m) and in one deeper sample from 2624 ft (820 m). It is possible that the mesoscopic records were influenced by discolorations due to hematite. On the other hand, the microscopic data reported are consistent with quantitative measurements (17) which identify ERDA #9 rock salt, 2036 – [illegible] ft (636 – [illegible] m) as more than 97 weight per cent water soluble with no more than 1.7% clay and silt. In samples from 2609 – 2618 ft (816 – 818 m) the water soluble content was > 98.[illegible]%. One specimen from 2705.4 ft (845 m) contained only [illegible]% water solubles with 0.65% sulfates and 4.14% primarily clay and quartz (17). Water insoluble residues were negligible in several specimens between 26[illegible] – [illegible].5 ft (815 – [illegible] m).

TEST MATRIX

The tests which are described in this report are listed in Table [illegible]. The tests shown are similar to those completed by RE/SPEC, Inc. for rock salt from the lower horizon of the WIPP study area (10, 11). However, instead of duplicating experimental conditions throughout for like core, most tests actually complement each other by virtue of overlapping but not necessarily identical parameter conditions. For example, earlier RE/SPEC experiments were carried out at principal stress differences of 1500, 3000 and 4,500 psi ([illegible], [illegible] and 31.0 MPa (10, 11)). The present tests on salt from below [illegible] ft ([illegible] m) were performed at approximately 1000, 2200 psi (6.9, [illegible] MPa), etc. Beyond this coordination of efforts there exist some important distinctions. The tests of this study provide data on rock salt from WIPP at depths [illegible] – 2100 ft ([illegible] – [illegible] m). Also, core from 2600 – [illegible] ft ([illegible] – [illegible] m) was tested at the low stress difference of 1000 psi (6.9 MPa) and up to a peak temperature of 200°C. Finally, larger samples were employed and the test durations were increased to an average of [illegible] hours per experiment. Both facts enhance the resolution of creep rates particularly around or below 10^{-9} s^{-1}.

TABLE 2

Creep Test Matrix

Specimen No.	$\sigma_1 - \sigma_3$ (psi)	(MPa)	σ_3 (psi)	(MPa)	T (°C)
Upper Level Rock Salt, Depth 2000-2100 ft (625-650 m)					
1	2000	13.8	500	3.5	22
	4500	31.0	500	3.5	22
2	3000	20.7	500	3.5	22
	4500	31.0	500	3.5	22
3	2000	13.8	3000	20.7	22
	4500	31.0	3000	20.7	22
4	3000	20.7	3000	20.7	22
	4500	31.0	3000	20.7	22
	3000	20.7	3000	20.7	22
Lower Level Rock Salt, Depth 2600-2800 ft (810-875 m)					
5	1000	6.9	500	3.5	22
	2200	15.2	500	3.5	22
	3300	22.8	500	3.5	22
	2200	15.2	500	3.5	22
6	1000	6.9	3000	20.7	22
7	1000	6.9	0	0	100
8	1000	6.9	500	3.5	100
9	1000	6.9	500	3.5	100
	2200	15.2	500	3.5	100
10	1000	6.9	3000	20.7	100
	2200	15.2	3000	20.7	100
11	1000	6.9	500	3.5	200
12	1000	6.9	3000	20.7	200
13	4500	31.0	500	3.5	22

RESULTS

Table 3 contains a summary of general statistics of all creep experiments, including stress states, test durations and numerically greatest axial and radial strains. The actual stresses which were attained here differ slightly from the target stresses in Table 2. The highest values of principal stress difference represent the following fractions of the ultimate stress values σ_u which were measured at a loading rate $d(\sigma_1 - \sigma_3)/dt$ = 30 – 60 psi/min (0.21 – 0.41 MPa/min) (Table 1):

$$(\sigma_1 - \sigma_3) = 0.66\sigma_u \text{ at } \sigma_3 = 500 \text{ psi } (3.5 \text{ MPa}),\ T = 22^\circ C$$

$$(\sigma_1 - \sigma_3) = 0.55\sigma_u \text{ at } \sigma_3 = 500 \text{ psi } (3.45 \text{ MPa}),\ T = 100^\circ C$$

$$(\sigma_1 - \sigma_3) = 0.43\sigma_u \text{ at } \sigma_3 = 500 \text{ psi } (3.45 \text{ MPa}),\ T = 200^\circ C$$

$$(\sigma_1 - \sigma_3) < 0.26\sigma_u \text{ at } \sigma_3 = 3000 \text{ psi } (20.7 \text{ MPa}),\ T = 22^\circ C$$

$$(\sigma_1 - \sigma_3) \leq 0.36\sigma_u \text{ at } \sigma_3 = 3000 \text{ psi } (20.7 \text{ MPa}),\ T = 200^\circ C$$

Fig. [illegible] shows typical records of $(\sigma_1 - \sigma_3)$ versus time. Relatively small cyclical variations in stresses are due to diurnal changes in the ambient laboratory temperature (± 0.5°C).

Test durations varied from as little as 80 hours in one experiment at 200°C to 1842 hours in an ambient temperature test. The average test duration was 665 hours.

Table 3 also lists the total axial and radial creep strains which were reached in each experiment. Throughout, strains are given as engineering strains, e.g. $\Delta L/L$, relative to the sample dimensions at the beginning of each test. Note that some radial strain data are marked as uncertain either because data analyses have not been completed or because they require additional checks. For the same reason the observed volumetric strains are described only in a semi-quantitative sense. Small amounts of compaction which are indicated in Table 3 may or may not prove to be real. In any event, the total volumetric creep corresponding to the first stages of tests 9-2083.5 are small ($\varepsilon > -1\%$). Generally, the same appears to apply to all tests where Table 3 now shows question marks.

TABLE 3

Summary Statistics of Creep Tests

Stress and strain represent true stress and engineering strain, respectively.

ϵ_1 : axial strain; ϵ_3 : radial strain; ϵ : volumetric strain. Parentheses denote uncertainties.

Question marks indicate that data are missing or not yet available.

Key - DDD : large dilatancy (> 4%); DD : considerable dilatancy (> 1%); D : some dilatancy (< 1%); C : some compaction (C).

Sample (Hole# - Depth (ft))	$\sigma_1 - \sigma_3$ (psi)	$\sigma_1 - \sigma_3$ (MPa)	σ_3 (psi)	σ_3 (MPa)	Temper. (°C)	Test Duration (Hrs)	(ϵ_1) max (%)	$(-\epsilon_3)$ max (%)	Direction of ϵ
Upper Level Salt									
9-2078	2000	13.8	500	3.5	22	310	.273	.169	0
9-2078	4500	31.0	500	3.5	22	166	7.18	4.57	DD
9-2083	2950	20.3	500	3.5	22	1238	2.22	1.68	DD
9-2083	4500	31.0	500	3.5	22	360	13.80	>9.58	DDD
9-2078.5	1700	11.7	3000	20.7	22	311	.125	(0.02)	?
9-2078.5	4100	28.3	3000	20.7	22	166	3.62	2.78	D
9-2083.5	2900	20.0	3000	20.7	22	1085	2.02	?	(C)
9-2083.5	4400	30.3	3000	20.7	22	1256	11.40	(>6.4)	(D)
9-2083.5	3000	20.7	3000	20.7	22	675	[illegible]	?	?
Lower Level Salt									
9-2625	1200	8.3	500	3.5	22	1842	.22	.08	0
9-2625	2200	15.2	500	3.5	22	1481	2.27	(1.30)	D
9-2625	3300	22.8	500	3.5	22	356	5.31	(2.28)	?
9-2625	2300	15.9	500	3.5	22	595	0.23	(0.07)	?
9-2677	1150	7.9	3000	20.7	22	671	[illegible]	(0.06)	(0)
9-2672.5	1000	6.9	30	0.2	100	612	2.44	?	?
9-2624	1050	7.2	500	3.5	100	652	2.79	[illegible]	-
9-2686	1000	6.9	500	3.5	100	747	[illegible]	0.47	(C)
9-2686	2350	16.2	500	3.5	100	490	17.6	11.40	DD
9-2671	930	6.4	3030	20.9	100	1174	0.98	[illegible]	[illegible]
9-2671	2250	15.9	3000	20.7	100	868	29.3	(>10.6)	D
9-2688	1000	6.9	530	3.7	200	[illegible]	6.48	[illegible]	D
9-2668	1000	6.9	3020	20.8	200	165	15.18	[illegible]	DD
9-2777	4800	33.1	500	3.5	22	[illegible]	[illegible]	14.5	DDD

The large values of dilatancy, $\epsilon < -4\%$, of experiments 9-2083, 9-2686, and 9-2777, are associated with accelerated creep and impending creep fracture. It should be noticed that the total axial and radial creep strains in the latter tests are bounded by fracture strain values which were measured in short-term, quasi-static tests into the post-failure regime.

Files of representative data for all experiments are compiled in an appendix. For the time being these files are restricted to axial strain time data (ϵ_1, t). Obviously, the number of data points (9 to 12) in these condensed files is much smaller than in the original files (typically 750). Indications of data scatter are included deliberately to demonstrate maximum variations in the creep records. These variations are caused simply by experimental scatter or by the number of updates of ram force (Fig. 2) to maintain a mean constant principal stress difference. The importance of these updates is particularly evident in Figs. 3 and 4 for specimen 9-2777. Here updates in ram force were delayed deliberately to establish likely differences in results between constant force tests and constant stress (creep) experiments. Clearly, these differences can be significant. Constant force tests may alter the course of primary creep at constant stress and may prevent the development of secondary creep altogether.

Figs. 5 through 12 contain examples of crossplots to explore the effects of principal stress difference, temperature and confining pressure. Indications of the reproducibility of results are provided by three sets of data, in Figs. 5 through 8 and in the digitized data files 9-2078/.5/22 and 9-2083/.5/22, 9-2078.5/3./22 and 9-2083.5/3./22 and 9-2624/.5/100 with 9-2686/.5/100 (Appendix). The large differences in results of experiments 9-2624/.5/100 and 9-2686/.5/100 are unexplained but deemed exceptional.

The comparisons in Figs. 5 through 12 assume that strain history has no major influence on creep as stress difference is increased. Therefore, no distinction was made between experiments which were performed on the same sample if the specimen was subjected to successively increasing levels of principal stress difference. Strain history effects with decreasing principal stress difference will be discussed later.

A cursory comparison of the results for rock salt from both horizons of interest to the WIPP (2000 – 2100 ft and 2600 – 2800 ft) indicates that trends in creep behavior are independent of depth. Therefore, the following discussions will not consider depth as a variable although the data pertaining to the upper and lower levels (Table 2) will not actually be mixed. The general agreement in results is consistent with the high purity of salt tested ([illegible]).

General Features

The crossplots, Figs. 5 through 12, demonstrate that New Mexico rock salt undergoes the three classical stages of creep: primary (transient) creep, secondary (steady state) creep and tertiary (accelerated) creep which terminates in creep fracture. Limited radial strain data (Figs. 6 and 8) further indicate that creep appears to proceed with little change in rock volume at low principal stress difference, small strains and/or high temperature. In turn, noticeable dilatancy develops as $(\sigma_1 - \sigma_3)$ is raised. Eventually large amounts of dilatancy (damage) led into creep fracture.

In a qualitative sense the creep data shown verify the well known nonlinear effects of principal stress difference and temperature (Figs. [illegible] through 12). On the other hand, first examinations in this study suggest that pressure is important only in the control of tertiary creep and creep fracture.

Periodic measurements on deformed samples after testing led to the conclusion that essentially all creep strain was irreversible. This conclusion was strengthened by monitoring the axial and radial dimensions of two specimens continuously for periods of twenty days. No recovery was resolved either by means of dial gauges (axial strain) or by means of strain gauge instrumented clip-on gauges (radial strain).

Primary (Transient) Creep

Efforts were initiated to describe primary creep of New Mexico rock salt objectively. Preliminary work consisted of fitting axial strain-time data (ϵ_1, t) to logarithmic and power relations of the form

$$\epsilon_p' = A \log(t) \qquad (i)$$

$$\epsilon_p'' = Ct^n \qquad (ii)$$

where A, C, and n are constants. Typical log-log and semi-log plots of the data are given in Figs. 15 and 16. Although the foregoing equations are empirical they have been used widely and often provide excellent approximations to experimental data at constant stress. These equations are not constitutive equations, and it is recognized that equations (i) and (ii) predict infinite strain rates at zero time. Obviously the interpretation of Figs. 15 and 16 requires considerable judgment. For this preliminary analysis two assumptions were made which permit comparisons of the present results among one another and with published primary creep data for rock salt. First, primary creep, ϵ_p and secondary creep ϵ_{ss}, proceed simutaneously such that $\epsilon_{total} = \epsilon_p + \epsilon_{ss}$ (18). It was also assumed that total creep is governed by primary creep at less than approximately 60 hours.

In some cases (Fig. 16) it appeared that primary creep might be described best as lagarithmic creep. However, in the majority of experiments maximum statistical correlations were obtained by means of power relations which are summarized in Table 4 in terms of the "constants" C and n. For the sake of

TABLE [illegible]

[illegible] of Primary (Transient) Creep Data According
to Data Fit of Type $\epsilon_1 = Ct^n$(in/in); t : time (s); i = a, b
Stress and strain represent true stress and engineering strain, respectively.

Sample	$\sigma_1 - \sigma_3$		σ_3		T			Strain Measures at 100 hrs	
(Hole# - Depth)	(psi)	(MPa)	(psi)	(MPa)	(°C)	C	n	ϵ_1 (%)	ϵ_i/ϵ_i
				Upper Level Salt					
9-2078	2000	13.8	500	3.5	22	[illegible].16E-4	[illegible].133	[illegible]	[illegible]
9-2078	4500	31.0	500	3.5	22	[illegible]	[illegible]	[illegible].17	[illegible]
9-2083	2950	20.3	500	3.5	22	[illegible]	[illegible].185	[illegible]	[illegible]
9-2083	4500	31.0	500	3.5	22	6.68E-5	[illegible]	5.0[illegible]	48.[illegible]
9-2078.5	1700	11.7	3000	20.7	22	1.5[illegible]E-4	[illegible].146	0.1[illegible]= ϵ_a	1.[illegible]
9-2078.5	4100	28.3	3000	20.7	22	3.3[illegible]E-4	[illegible]	[illegible].68	[illegible]
9-2083.5	2900	20.0	3000	20.7	22	1.4[illegible]E-3	0.138	[illegible]	[illegible].4
9-2083.5	4400	30.3	3000	20.7	22	[illegible]	.345	[illegible]	[illegible]
9-2083.5	3000	20.7	3000	20.7	22	-	-	-	-
				Lower Level Salt					
9-2625	1200	8.[illegible]	[illegible]	3.5	22	[illegible]	[illegible]	[illegible].123= ϵ_b	1.[illegible]
9-2625	2200	15.2	5[illegible]	3.5	22	1.[illegible]	[illegible]	.76	6.2
9-2625	3300	22.[illegible]	500	3.5	22	1.41E-4	[illegible].400	2.64	21.5
9-2625	2300	15.[illegible]	500	3.5	22	-	-	-	-
9-2677	1150	7.9	3000	20.7	22	[illegible]	[illegible]	.1[illegible]	[illegible]
9-2672.5	1000	6.[illegible]	[illegible]	[illegible]	[illegible]	1.38E-[illegible]	[illegible]	[illegible]	[illegible]
9-2624	[illegible]	[illegible]	[illegible]	[illegible]	[illegible]	[illegible]	[illegible]	[illegible]	[illegible]
9-2686	[illegible]	[illegible]	[illegible]	[illegible]	[illegible]	[illegible]	[illegible]	[illegible]	[illegible]
9-2686	[illegible]	[illegible]	[illegible]	[illegible]	[illegible]	[illegible]	[illegible]	[illegible]	[illegible]
9-2673	[illegible]	[illegible]	[illegible]	[illegible]	[illegible]	[illegible]	[illegible]	[illegible]	[illegible]
9-2671	[illegible]	[illegible]	[illegible]	[illegible]	[illegible]	[illegible]	[illegible]	[illegible]	[illegible]
9-26[illegible]	[illegible]	[illegible]	[illegible]	[illegible]	[illegible]	[illegible]	[illegible]	[illegible]	[illegible]
9-2668	[illegible]	[illegible]	[illegible]	[illegible]	[illegible]	[illegible]	[illegible]	[illegible]	[illegible]
9-[illegible]	[illegible]	[illegible]	[illegible]	[illegible]	[illegible]	[illegible]	[illegible]	[illegible]	[illegible]

consistency all fits were made within the time interval $1 \le t$ (hrs) $\le$ 55. With three exceptions the selection of this time interval ensured the highest correlations between actual data and the approximations by means of equation (11). Combinations of logarithmic and power creep, e.g. $\varepsilon_p = \varepsilon_p' + \varepsilon_p''$, are possible but have not yet been considered in detail.

Although further analyses are needed, two observations deserve mentioning. (1) If a "power law" creep formulation is accurate for constant stress, then the multiplier C and the time exponent n appear to be variable. According to Table 4, n increases up to a factor of five with increases in principal stress difference and temperature. Considerable differences in the values of n remain even if allowances are made for the influence of secondary creep particularly at elevated temperature. More work is needed to determine whether the parameters C and n are independent of one another. Coupling between C and n was indicated by some earlier data for artificial and natural rock salt (3, 10, 11). (2) The influence of confining pressure on axial creep (ε_1, t) appears to be small, particulary at low $(\sigma_1 - \sigma_3)$. This follows from comparisons of the empirical variables C and n. It also follows from a comparison of normalized axial strain data, $\varepsilon_1/\varepsilon_i$, which were calculated from $\varepsilon_1 = C t^n$ at t = 100 hours (Table 4). However, caution should be exercised in generalizing this result to shear strain $(\varepsilon_1 - \varepsilon_3)$, i.e. before considering further the nature of radial creep.

Secondary (Steady State) Creep

The existence of secondary creep is difficult to establish wihhout doubt. In this case, estimates of secondary creep rates in Table 5 are based on two criteria. First, plots had to contain what "looked like" straight line portions. More objectively, it was required that the slope r of plots in the space $\log(\varepsilon_{total})$, $\log(t)$ increased with time from the value r = n during primary

TABLE 5

Summary of Secondary Creep Estimates
(Parentheses denote upper bound values)
Stress and strain represent true stress and engineering strain, respectively.

Sample (Hole# - Depth (ft))	$\sigma_1 - \sigma_3$ (psi)	$\sigma_1 - \sigma_3$ (MPa)	σ_3 (psi)	σ_3 (MPa)	Temper. (°C)	Estimated Secondary Creep Rate $\dot{\varepsilon}_1 (10^{-8}/s)$
			Upper Level Salt			
9-2078	2000	13.8	500	3.5	22	(0.042)
9-2075	4500	31.0	500	3.5	22	(5.02)
9-2083	2950	20.3	500	3.5	22	(0.16)
9-2083	4500	31.0	500	3.5	22	(5.8)
9-2078.5	1700	11.7	3000	20.7	22	(0.012)
9-2078.5	4100	28.3	3000	20.7	22	(2.25)
9-2083.5	2900	20.0	3000	20.7	22	(0.23)
9-2083.5	4400	30.3	3000	20.7	22	(1.10)
9-2083.5	3000	20.7	3000	20.7	22	0.018
			Lower Level Salt			
9-2625	[illegible]	8.3	500	3.5	22	(0.014)
9-2625	[illegible]	15.2	500	3.5	22	(0.20)
9-2625	[illegible]	[illegible]	500	3.5	22	(1.93)
9-2625	[illegible]	15.9	500	3.5	22	(0.033)
9-2677	1150	7.9	3000	20.7	22	(0.008)
9-2672.5	[illegible]	6.9	30	0.2	100	1.00
9-2628	[illegible]	7.2	500	3.5	100	0.81
9-2686	[illegible]	[illegible]	[illegible]	3.5	100	[illegible]
9-2686	[illegible]	[illegible]	[illegible]	[illegible]	[illegible]	[illegible]
9-2671	[illegible]	[illegible]	3000	[illegible]	100	[illegible]
9-2671	[illegible]	[illegible]	3000	20.7	100	[illegible]
9-2688	[illegible]	[illegible]	[illegible]	3.7	200	[illegible]
9-2668	[illegible]	[illegible]	3000	20.7	200	[illegible]
9-2777	[illegible]	33.1	500	3.5	22	[illegible]

creep (Table 4) towards $r = 1$ when secondary creep becomes overriding. For $\varepsilon_{total} = \varepsilon_{t} + \varepsilon_{ss}$, rising values of r indicate that the contribution of secondary creep to the total creep strain is increasing. If the second criterion was not satisfied clearly, estimates of creep rates in Table 5 are the smallest observed creep rates at the end of each test. Hence, they only constitute upper bounds and are listed in parentheses.

To compare the secondary creep results of New Mexico rock salt quickly, the assumptions were made that the total creep is thermally activated, that the effects of stress, temperature and pressure are separable and that the temperature dependence can be described by a single activation energy. It was further stipulated that secondary creep rates are proportional to a power function of stress (18-20). Then, following standard procedures the graphs of Figs. 17 - 1[illegible] were constructed for upper and lower level salt. Figs. 17 and 18 include data for 2 in. diameter samples of RE/SPEC, Inc. (10, [illegible]). Neglecting the uncertainties in some of the results in parentheses, estimated values of activation energy fall into the relatively narrow range between Q = [illegible] kcal/mole and Q = 13.[illegible] kcal/mole. The number of data available does not suffice to determine possible variations in Q with temperature. A pressure effect is weak if it is present at all.

Stress exponents of the results in Table 5 are listed in Figs. 18 and 19 for both salt horizons considered. Keeping different groups of tests deliberately apart, the stress exponents vary considerably between 3.1 and 6.5 depending on temperature and which results are included in a particular linear data fit. Well defined secondary creep rates correspond to m = 3.1 at 100°C. The remaining values only correspond to secondary creep estimates (smallest observed creep rates).

Tertiary Creep and Creep Fracture

Tertiary creep was measured in four experiments at 500 psi (3.5 MPa) confining pressure and T = 22°C and at T = 100°C with confining pressures of

0, 500 and 3000 psi (0, 3.5, 20.7 MPa). Except in one case, σ_3 = 3000 psi (20.7 MPa; sample 9-2671), tertiary creep terminated in creep fracture associated with a considerable amount of dilatancy much like that which is measured at the ultimate stress in quasi-static tests. At 3000 psi (20.7 MPa) accelerated creep started at $\varepsilon_1 \approx 13.5\%$ and continued to $\varepsilon_1 \approx 29\%$ over several hundred hours and with an approximately 10-fold increase in creep rate. However, no fracture was imminent at the peak strain before the experiment was terminated for inspection of the specimen.

Effect of Stress or Strain History

It was stated in an earlier section that the data representations of Tables 4 and 5 implied no effect of stress or strain history under increasing stress difference. This assumption appears acceptable in the light of published creep results (5, 10, 11) but questionable in view of recent short-term data for variable stress paths which may or may not be relevant for creep (12). To evaluate the influence of more complicated histories and partly to check the accuracy of some secondary creep rates in Table 5, two sets of tests were performed in successive stages of increasing and decreasing stress. For one experiment (9-2683.5; Fig. 13) the principal stress difference was changed from 3000 psi (20.7 MPa for 1088 hours) to 4400 psi (30.3 MPa for 1256 hours) and back to 3000 psi (20.7 MPa for 675 hours). In the second experiment (9-2625; Fig. 14) ($\sigma_1 - \sigma_3$) was varied from 2200 psi (15.2 MPa for 1481 hours) to 3300 psi (22.7 MPa for 356 hours) and again to 2300 psi (15.9 MPa for 595 hours). Details of these tests are listed in Tables 3-5. The most important result is that the estimated secondary creep rates at approximately 3000 psi (20.7 MPa) and 2300 psi (15.9 MPa) dropped by nearly one order of magnitude after creep had occurred at higher values of principal stress difference, i.e., 4400 (30.3 MPa) and 3300 psi (22.7 MPa), respectively (stages C2 and C3 in the captions of Figs. 13 and 14).

PRELIMINARY COMPARISON OF RESULTS WITH RE/SPEC DATA AND DISCUSSION

In view of limited data and data scatter it is important to compare the present results with the results of RE/SPEC Inc. (10, 11). Given the complementary nature of all tests, satisfactory agreement would automatically broden the overall data base available for constitutive modeling and model validation.

Qualitatively, available results demonstrate that New Mexico rock salt undergoes all stages of creep from primary creep through creep fracture. More important, all of these stages were observed at levels of stress and temperature which are of interest to the WIPP. This means that past modeling efforts which have concentrated on the prediction of primary creep must be extended.

Primary and secondary creep are recognized readily in a qualitative sense. However, the combined data of Sandia and RE/SPEC Inc. indicate independently that unambiguous descriptions of these phenomena are difficult. Particular difficulties arise because primary and secondary creep appear to be overlapping, because primary creep at small time probably depends upon the initial loading rate and because most secondary creep rates are only upper bounds. As a result, the description of primary creep in terms of power creep, for example (Table 4), is sensitive to the time interval which is chosen to fit the experimental data in the space log (ε_1), log(t). Furthermore, the power creep relation which was used here renders poor fits to experimental measurements at times less than approximately one hour. At elevated temperature primary creep interpretations are distorted by fast secondary creep which is going on simultaneously. Whatever the reason, ambiguities in the interpretation of creep data probably produced errors in description and predictions. For example, based on Tables 4 and 5 the predicted total axial creep strain for sample [illegible]-2671, $(\sigma_1 - \sigma_3)$ = 2250 psi (15.5 MPa) is 16.3% after 500 hours if $\varepsilon_{total} = \varepsilon_p + \varepsilon_{ss}$ as suggested by the nature of double logarithmic plots. This value overpredicts the actual strain accumulation (ε_1 = 12.5%) after that time by approximately 30%.

Some qualitative disagreement between various sets of results arises concerning the influence of pressure. Available data (11, 12) led to the common conclusion that pressure enters as a first order effect into the prediction of tertiary creep and creep fracture. However, preliminary analyses of the present results suggest that the influence of pressure on transient and steady state creep is negligible. This observation runs contrary to earlier RE/SPEC data and to the results of short-term (quasi-static) experiments. To clarify this point more detailed examinations should be made of existing radial strain data. Also, further tests should be conducted particularly below 500 psi (3.5 MPa) confining pressure.

Preliminary quantitative comparisons of Sandia and RE/SPEC data are not totally satisfactory. One power creep description of RE/SPEC Inc. (11) appears to predict considerably larger creep strains than those which are indicated by the results of Table 4 and 5. For example, for primary creep periods of 100 hours several predictions at common stresses and temperatures differ by factors of approximately ten. RE/SPEC results also suggest higher secondary creep rates. However, it is emphasized that most of these comparisons have been carried out quickly and require checks and confirmation. Some of the observed differences might be due to specimen size. Values of average activation energies are relatively consistent and fall into the range $7.3 \leq Q \leq 13.9$ kcal/mole (Fig. 17). The majority of data fit $Q \approx 13.3$ kcal/mole.

It is not clear at this point how serious the observations of history effects might be if they are proven typical under decreasing principal stress difference. However, history effects might influence stress calculations and therefore affect the likelihood of creep fracture.

Tertiary creep and triaxial creep fracture developed at 200°C and surprisingly low values of principal stress difference ($\sigma_1 - \sigma_3 \approx 2300$ psi (15.9 MPa) even at $\sigma_3 \geq 500$ psi (3.5 MPa) confining pressure. Although these stresses and temperatures are likely to develop only very locally (21), the phenomena are significant enough to require additional study. For lack of established theories it will be necessary in part to conduct very long experiments. However, creep fracture predictions may also be aided by empirical correlations between creep fracture stress and quasi-static complete stress-strain characteristics (22, 23). Triaxial tests on granite, sandstone and marble suggested that complete quasi-static stress-strain records can be used to establish loci of limiting stable creep strains. Specifically, it appears that the total nonelastic (time-dependent) strain at any stress will not exceed the nonelastic strain to fracture at the same confining pressure and principal stress difference in quasi-static tests. Although this procedure is strictly empirical it appeals to the notion that nonelastic strains are a measure of damage and that the limiting strain establishes a maximum amount of damage as a function of stress state before an instability occurs with associated loss in load bearing ability. The foregoing empirical predictive scheme for creep fracture is invoked here because it correlates remarkably well with the available creep fracture observations in this report.

SUMMARY

An interim summary of triaxial creep experiments on rock salt was presented which were carried out at Sandia Laboratories in support of the proposed Waste Isolation Pilot Plant (WIPP) in southeastern New Mexico. Tests were performed on relatively large samples measuring 3.9 in (9.9 cm) diameter. Details of relevant experimental procedures and measurements were described. Results shown include digital data in condensed data files and numerous graphical comparisons for rock salt from two horizons 2000 – 2100 ft and 2660 – 2870 ft (610 – 640 m; 810 – 875 m) as a function of principal stress difference, temperature and confining pressure. Qualitative examinations showed that the rock salt exhibited all known stages of creep, i.e. primary, secondary and tertiary creep followed by creep fracture.

Preliminary evaluations of axial strain time records during primary creep (ε_1, t) are discussed assuming the applicability of so-called power "law" creep but without implying that the conventional power relationship is a constitutive equation. Contrary to earlier results, the primary creep data of this study appear to be independent of pressure within fairly wide experimental scatter. Estimates of steady state creep rates of interest to the WIPP vary from $\dot{\varepsilon}_1 < 10^{-10}\ s^{-1}$ to approximately $10^{-8}\ s^{-1}$. Tertiary creep and creep fracture were observed at ambient temperature and at 100°C. Creep fracture was not observed in a limited number of experiments at 200°C and is deemed unlikely except, possibly, at very low confining pressure, $\sigma_3 \leq 100$ psi (0.7 MPa). To predict creep fracture the use of an empirical procedure was suggested which correlates permanent time-dependent strains (damage) with limiting damage which is established from complete quasi-static stress-strain curves including pre- and post-failure records.

The analysis of tests which are described is continuing and includes examinations of existing radial strain data. It also includes a definitive comparison of data with earlier results of RE/SPEC Inc. beyond a cursory comparison which is included in this report.

ACKNOWLEDGMENTS

Mr. Steven Cave wrote software to curve fit the experimental data and provided all condensed data files in the appendix. Mr. Seyfred Toledo was helpful in specimen preparation and equipment maintenance.

REFERENCES

1. Schmidt, W., "Festigkeit und Verfestigung von Steinsalz," Zeitschr. Angew. Min., 1, 1, 1937.

2. U. S. Corps. of Engineers, "Project Dribble, Petrographic Examination and Physical Tests of Cores, Tatum Salt Dome, Mississippi," Army Engineers Waterways Experiment Station, Techn. Rep. No. 6-614, 1963.

3. Le Comte, P., "Creep of Rock Salt," J. Geol., 73, 469, 1965.

4. Höfer, K. H. and K. Thoma, "Triaxial Tests on Rock Salt," Int. J. Rock Mech. Min. Sci., 5, 195, 1968.

5. Lomenick, T. F., "Laboratory Pillar Model Experiments," in "Project Salt Vault: A Demonstration of the Disposal of High-Activity Solidified Wastes in Underground Salt Mines," Report, ORNL-4555, Oak Ridge Nat. Lab., 1971.

6. Dreyer, W., The Science of Rock Mechanics, Trans. Tech. Publ., 1972.

7. Serata, S., S. Sakuri and T. Adachi, "Theory of Aggregate Rock Behavior Based on Absolute Three-Dimensional Testing (ATT) of Rock Salt," in Basic and Applied Rock Mechanics, Proc. 10th U. S. Symp.

8. Menzel, W. and W. Schreiner, "Zum Geomechanischen Verhalten von Steinsalz verschiedener Lagerstätten der DDR, Teil II: das Verformungsverhalten," Neue Bergbautechnik, 7, 585, 1977.

9. Hansen, F. D. and I. F. Mirk, "Design Aspects of the Alpha Repository: III Uniaxial Quasi-Static and Creep Properties of the Site Rocks," Techn. Memor. Rep. RSI-0029, 1975.

10. Hansen, F. D., "Triaxial Quasi-static Compression and Creep Behavior of Bedded Salt from Southeastern New Mexico," Tech. Memor. Rep. RSI-0055, RE/SPEC, Inc., 1977.

11. Hansen, F. D. and K. D. Mellegard, "Creep Behavior of Bedded Salt from Southeastern New Mexico at Elevated Temperature," Techn. Memor. Rep. RSI-0062, RE/SPEC, Inc., 1977.

12. Wawersik, W. R. and D. W. Hannum, "Mechanical Behavior of New Mexico Rock Salt in Triaxial Compression Up to 200°C," J. Geophy. Res. (in press).

13. Griswold, G. B., "The Selection and Evaluation Studies of the Waste Isolation Pilot Plant (WIPP), Los Medanos, Eddy County, New Mexico," SAND77-0394б, Sandia Laboratories, 1977.

14. Wawersik, W. R., "Technique and Apparatus for Strain Measurements on Rock in Constant Confining Pressure Experiments," Rock Mech., 7, 231, 1975.

15. Wawersik, W. R., "Indirect Deformation (Strain) Measurements and Calibrations in Sandia Triaxial Apparatus for Rock Testing to 250°C," SAND79-0114, Sandia Laboratories, 1979.

16. Callender, J. F. and T. Ingwell, "Structural Petrology of Undeformed and Experimentally Deformed Halite Samples from USERDA Site #7 and #9," Report, Sandia Contract No. 05-7442, Department of Geology, University of New Mexico, 1977.

17. Powers, D. W. et. al., "Geological Characterization Report, Waste Isolation Pilot Plant (WIPP) Site, Southeastern New Mexico," Vol. II, SAND78-1596, Sandia Laboratories, 1978.

18. Carter, N. L. and S. H Kirby, "Transient Creep and Semibrittle Behavior of Crystalline Rocks," Pageoph, 116, 807-839, 1978.

19. Munson, D. E., "Preliminary Deformation Mechanism Map for Salt (With Application to WIPP), SAND79-0076, Sandia Laboratories, 1979.

20. Carter, N. L., "Steady State Flow of Rocks," Rev. Geophys. Space Phys., 14, 301-360, 1976.

21. Dawson, P. R., Personal Communication, Sandia Laboratories, 1978.

22. Wawersik, W. R. and W. S. Brown, "Creep Fracture of Rock in Uniaxial Compression," UTEC ME71-242, University of Utah, 1971.

23. Wawersik, W. R. and W. S. Brown, "Creep Fracture of Rock," UTEC ME73-197, University of Utah, 1973.

FIGURES

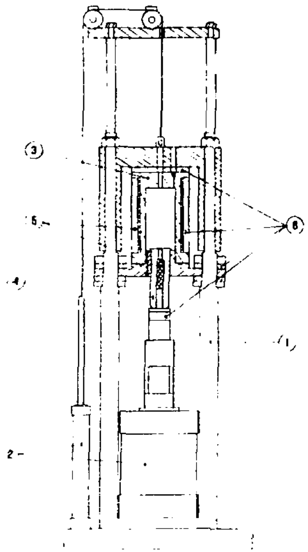

Fig. 1

Triaxial compression apparatus
Parts key: (1) load frame (2) hydraulic actuators
(3) pressure vessel (4) loading ram (5) heaters
(6) insulation

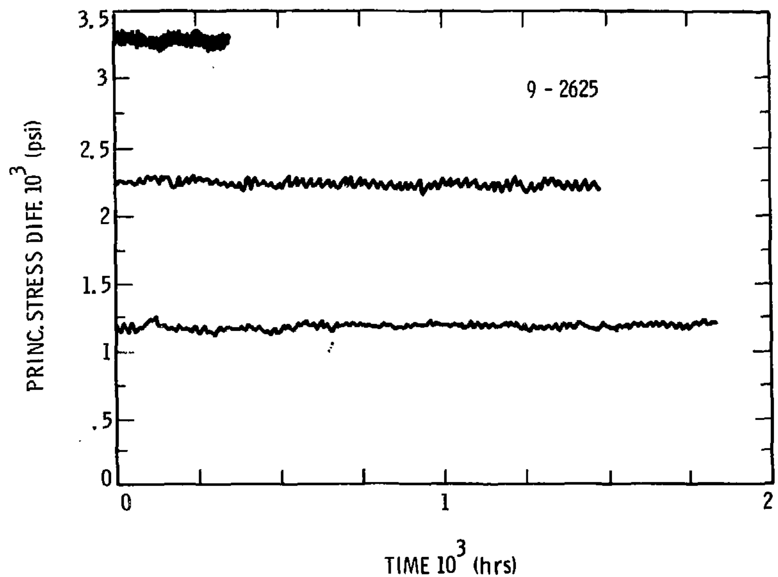

Fig. 2

Typical variations of principal stress difference with time for creep tests at 500 psi (3.5 MPa) confining pressure (Sample 9-2625).

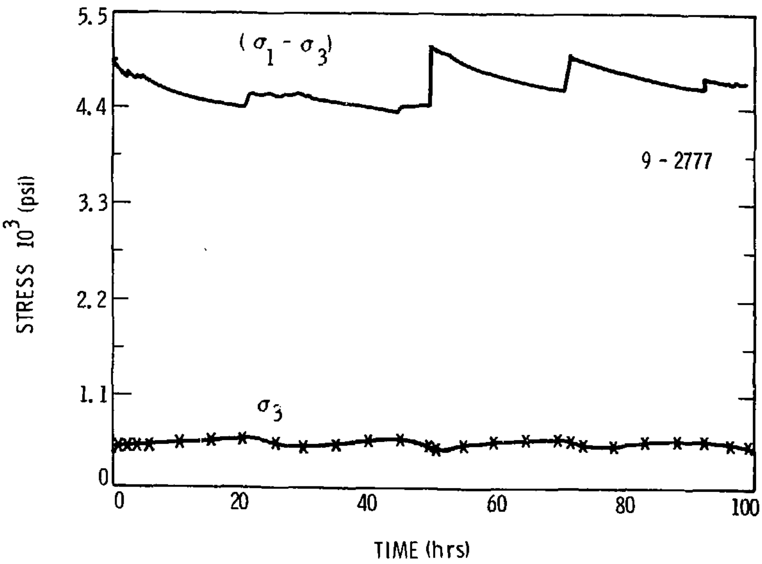

Fig. 3

Plot of principal stress difference and confining pressure versus time for sample 7-2777. Note extreme variations in $(\sigma_1 - \sigma_3)$ during periods of constant applied ram load (Fig. 1).

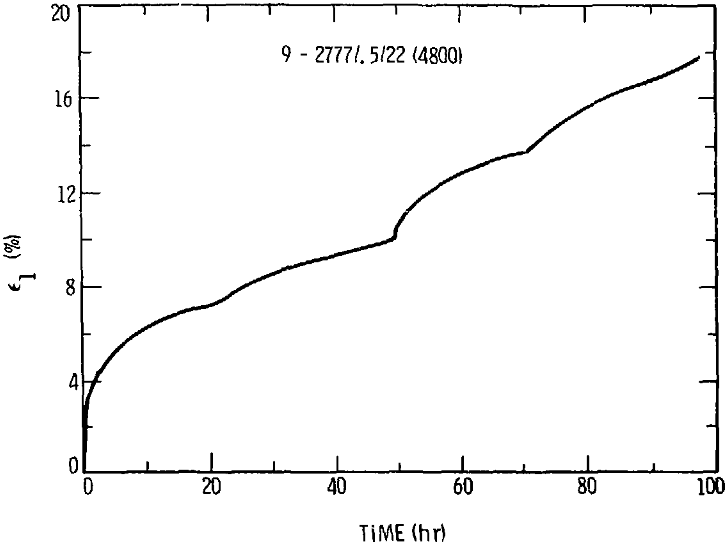

Fig. [illegible]

Axial creep record (ϵ_1 vs. t) for sample 9-2777. Note strong influence of updates in $(\sigma_1 - \sigma_3)$.

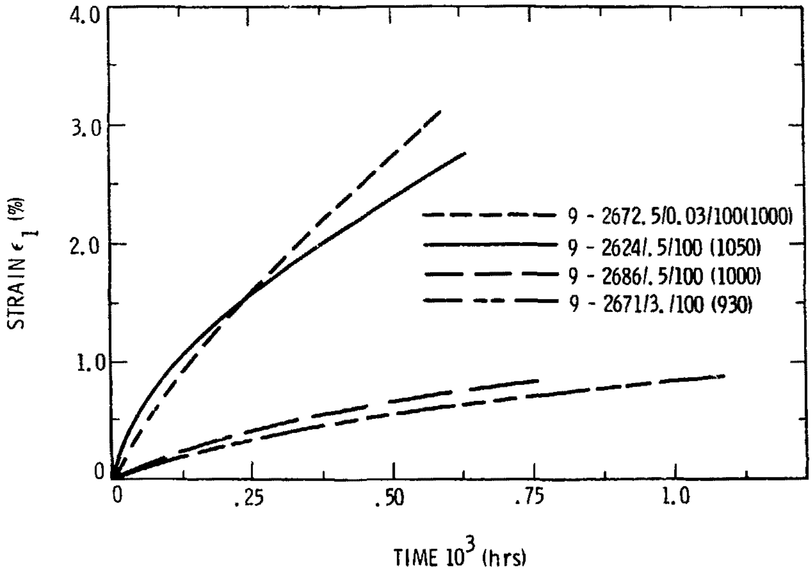

Fig. [illegible]

Axial creep response [illegible] at [illegible] psi [illegible] MPa), T = [illegible]°C and variable confining pressure. Note abbreviated test code: drillhole no.-core depth in ft/confining pressure in ksi/test temperature in °C (principal stress difference in psi).

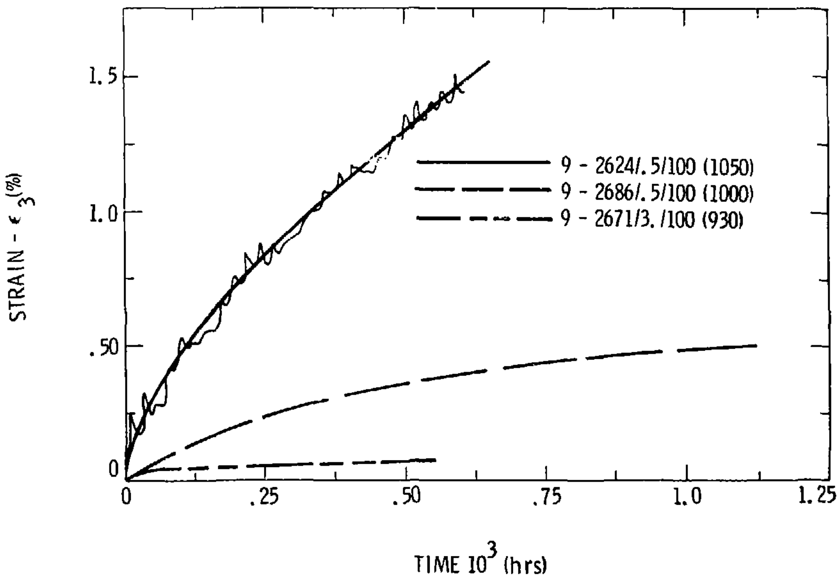

Fig. 6

Radial creep records ($-\epsilon_3$ vs. t) at ($\sigma_1 - \sigma_3$) = 1000 psi (6.9 MPa), T = 100°C and variable confining pressure (for test code see Fig. 5).

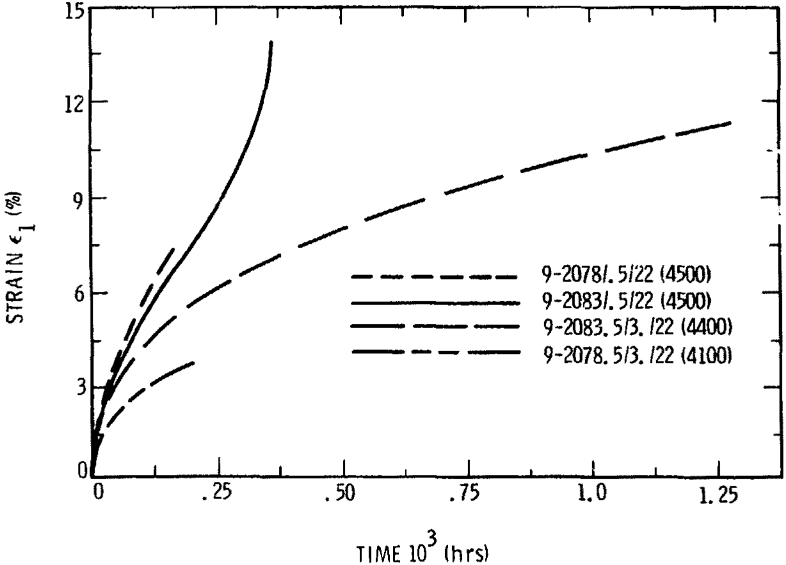

Fig. 7

Axial creep records (ϵ_1 vs. t) at $(\sigma_1 - \sigma_3)$ = 4500 psi (31.0 MPa), T = 22°C and <u>variable confining pressure</u> (for test code see Fig. 5).

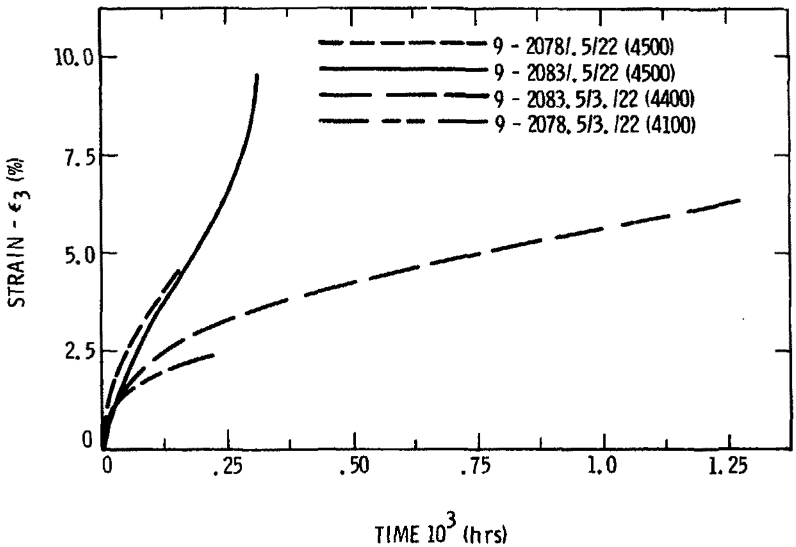

Fig. 8

Radial creep records ($-\varepsilon_3$ vs. t) at ($\sigma_1 - \sigma_3$) = 4500 psi (31.0 MPa), T = 22°C and <u>variable confining pressure</u> (for test code see Fig. 5).

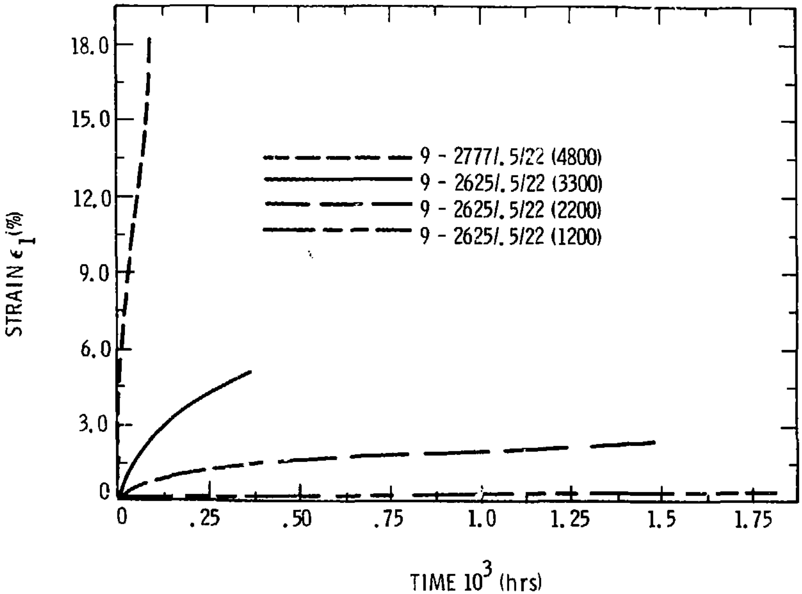

Fig. 9

Axial creep records (ε_1 vs. t) at σ_3 = 500 psi (3.5 MPa), T = 22°C and <u>variable principal stress difference</u> (for test code see Fig. 9).

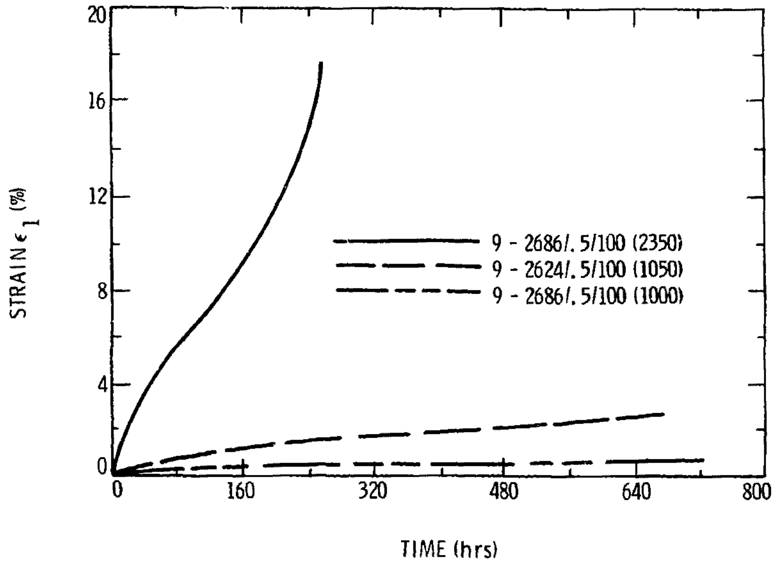

Fig. 10

Axial creep records (ϵ_1 vs. t) at σ_3 = 500 psi (3.5 MPa), T = 100°C and variable principal stress difference (for test code see Fig. 5).

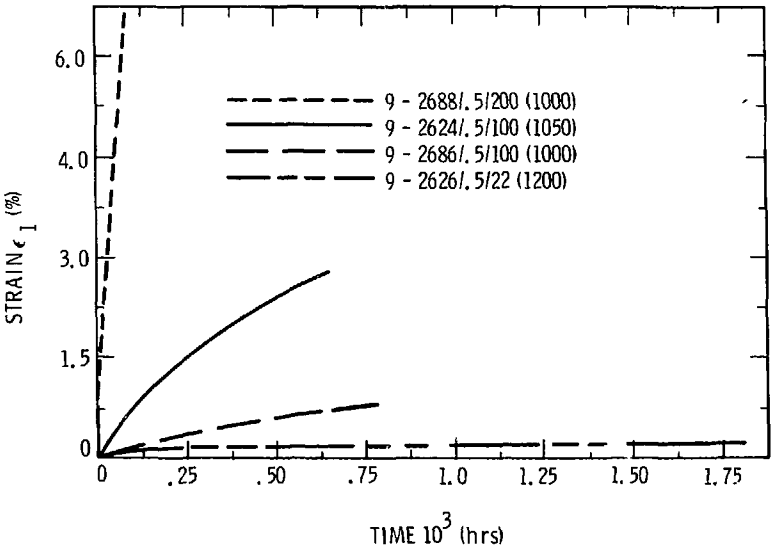

Fig. 11

Axial creep records (ϵ_1 vs. t) at σ_3 = 500 psi (3.5 MPa), (σ_1 - σ_3) = 1000 psi (6.9 MPa) and <u>variable temperature</u> (for test code see Fig. 5).

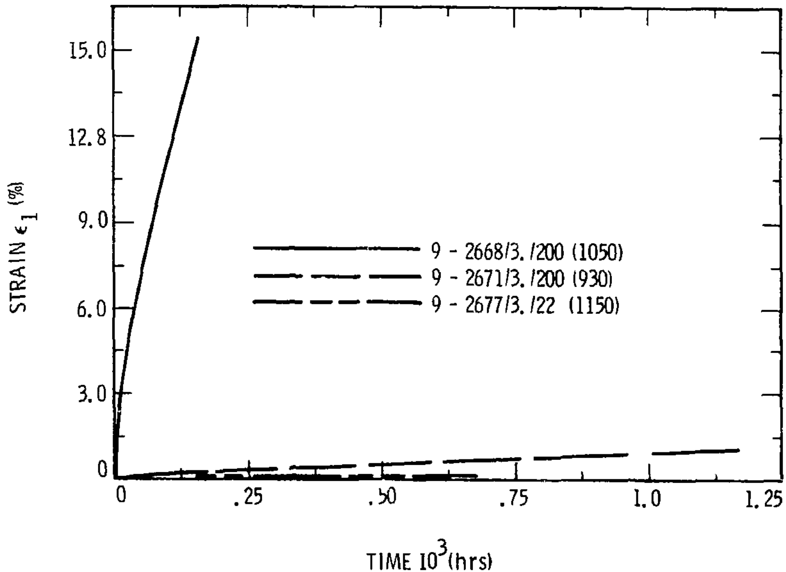

Fig. [illegible]

Axial creep records [illegible] at [illegible], [illegible] and <u>variable temperature</u> (for test code see Fig. [illegible]).

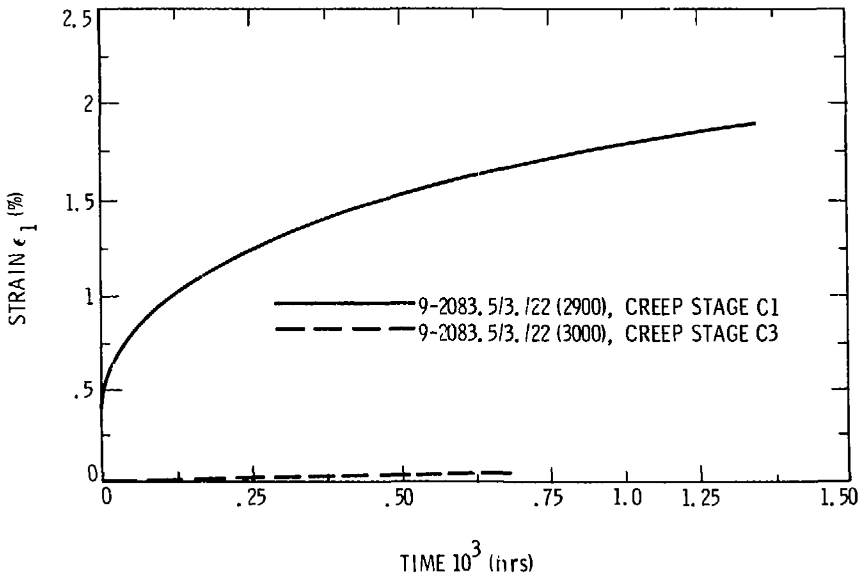

Fig. 13

Axial strain records (ϵ_1 vs. t) for sample [illegible]. Creep stage [illegible] proceeded at $(\sigma_1 - \sigma_3)$ = [illegible] psi ([illegible] MPa).

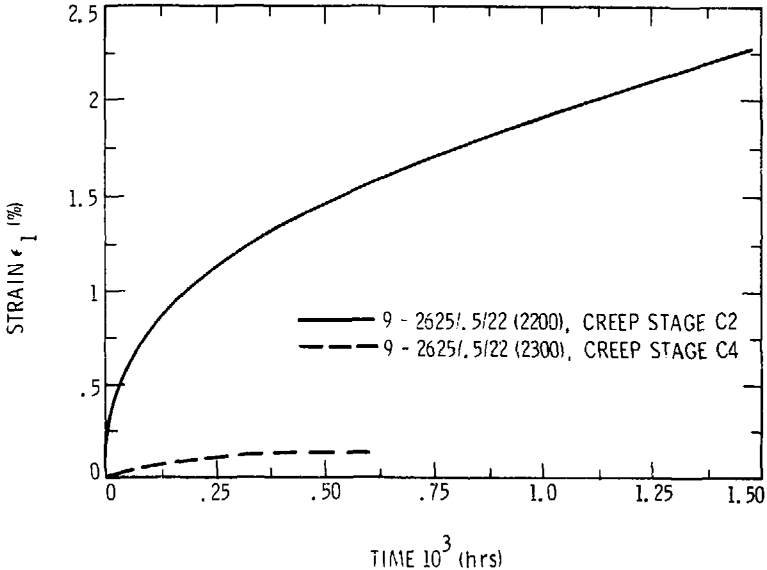

Fig. 1.

Axial strain records [illegible] vs. [illegible] for sample [illegible]. Creep stage [illegible] = [illegible] psi [illegible] MPa).

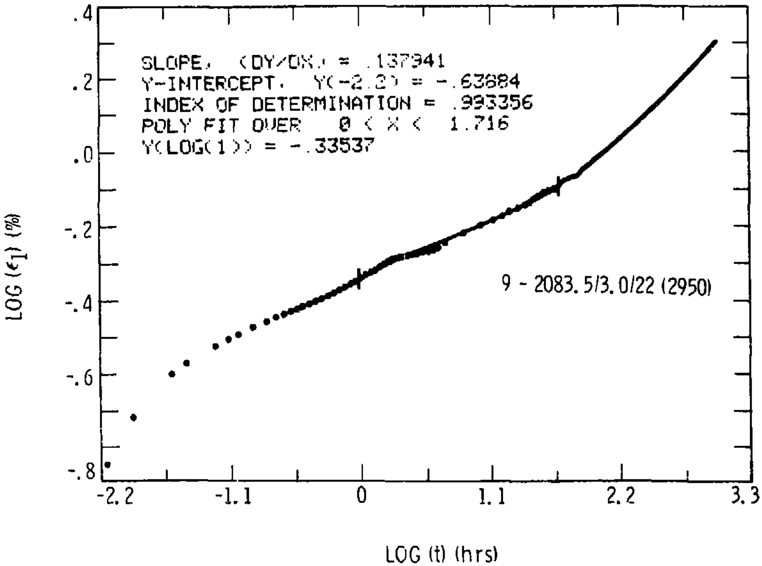

SLOPE, (DY/DX) = .137941
Y-INTERCEPT, Y(-2.2) = -.63684
INDEX OF DETERMINATION = .993356
POLY FIT OVER 0 < X < 1.716
Y(LOG(1)) = -.33537
9 - 2083.5/3.0/22 (2950)
LOG (ϵ_1) (%)
LOG (t) (hrs)
.4
.2
.0
-.2
-.4
-.6
-.8
-2.2
-1.1
0
1.1
2.2
3.3

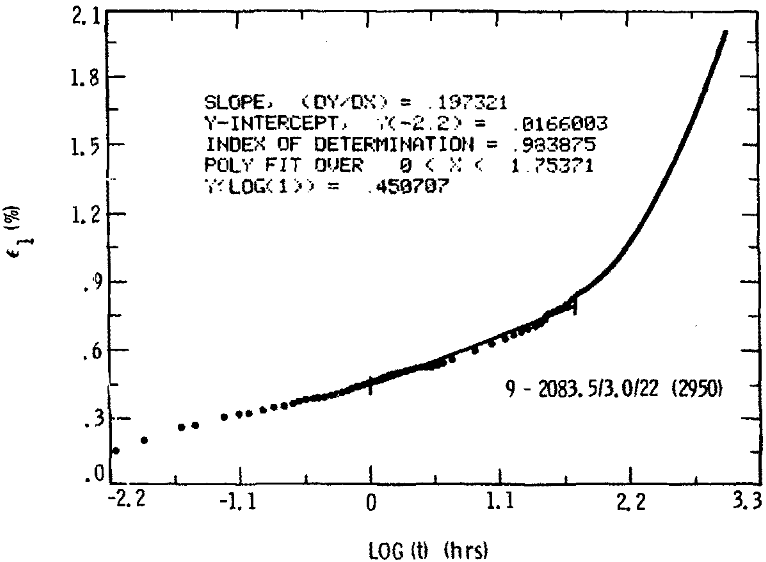

Fig. 16

Semi logarithmic plot ε_1 vs. log(t) of test 9-2803/.5/22 (2950)
(for test code see Fig. 5).

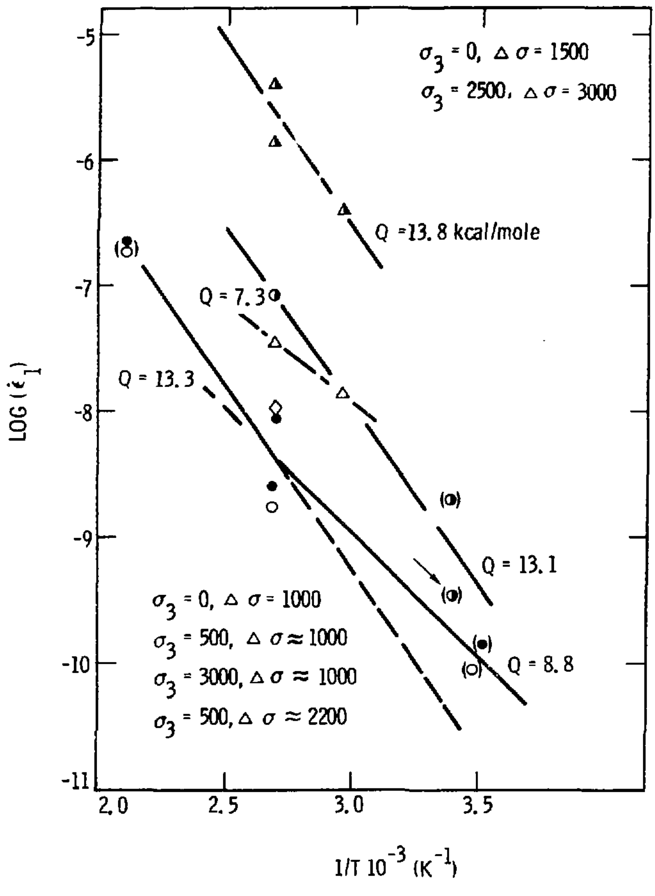

Fig. 17

Secondary creep rates $\dot{\varepsilon}_1$ for lower level salt in the space ($\log(\dot{\varepsilon}_1)$, 1/T). Triangular data points are due to RE/SPEC, Inc. (Ref. 11). $\Delta\sigma = (\sigma_1 - \sigma_3)$. Stresses are given in psi, strain rates in (s^{-1}). Parentheses denote upper bounds.

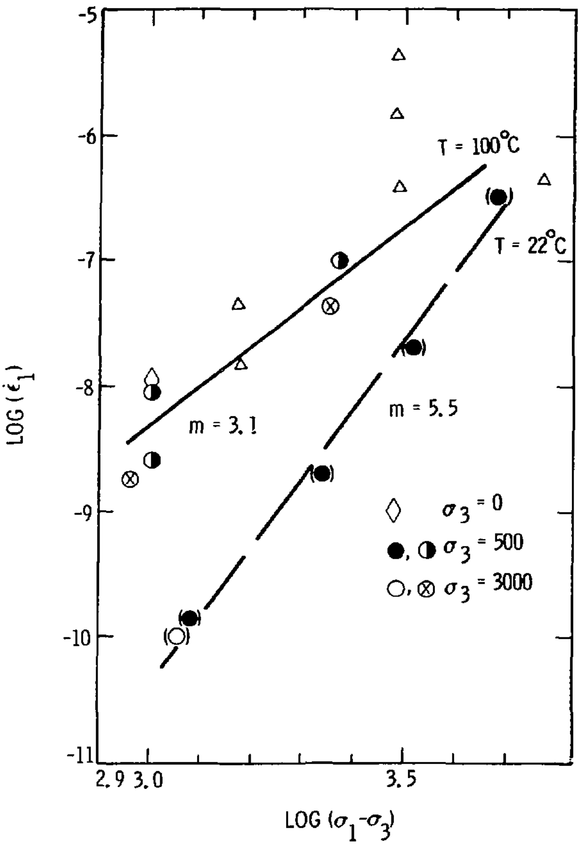

Fig. 18

Secondary creep rates $\dot{\varepsilon}_1$ in space $\log(\dot{\varepsilon}_1)$, $\log(\sigma_1 - \sigma_3)$ for lower level salt. Triangular data points are due to RE/SPEC, Inc. (Ref. 11). Stresses are given in psi, strain rates in (s^{-1}). Parentheses denote upper bounds.

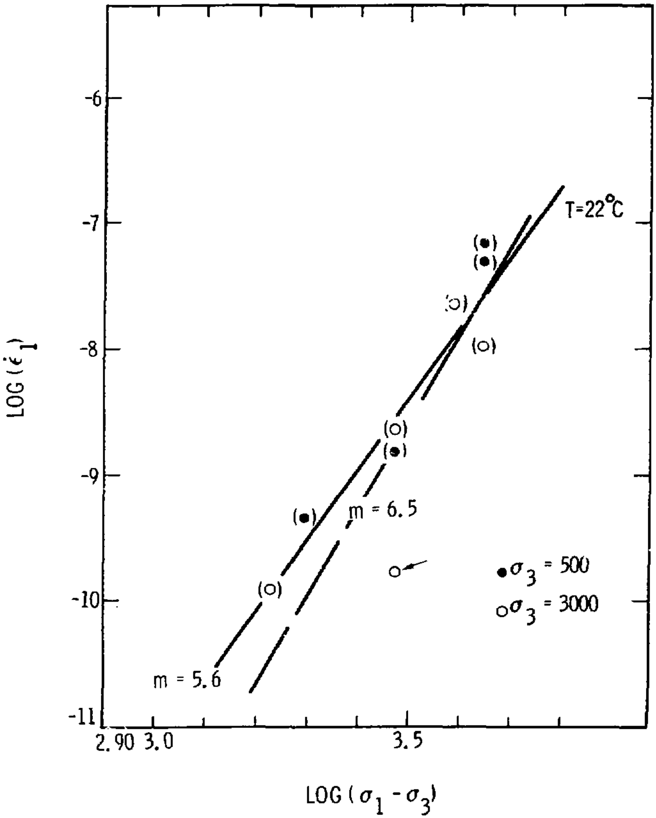

Fig. 10

Secondary creep rates $\dot{\varepsilon}_1$ in the space $\log(\dot{\varepsilon}_1)$, $\log(\sigma_1 - \sigma_3)$ for upper level salt. Stresses are given in psi, strain rates in (s^{-1}). Parentheses denote upper bounds.

APPENDIX

Listing of Representative, Condensed Creep Data Files. Note abbreviated test code (I.D.): Creep, stage no./drillhole no. - core depth in ft/confining pressure in ksi/test temperature in °C.

TEST I.D. C1/9-2078/.5/22

PRINC. STRESS DIFFERENCE 2000 PSI (13.8 MPA)

TIME (HRS)	E1 (%)
0	0
3.911	.152
8.889	.164
20.267	.174
24.889	.187
192.356	.25
227.556	.256
261.689	.262
284.089	.267
310.756	.272

TEST I.D. C2/9-2078/.5/22

PRINC. STRESS DIFFERENCE 4500 PSI (31.0 MPA)

TIME (HRS)	E1 (%)
0	0
8.2	1.822
24	2.63
33.4	3.42
45	3.867
61	4.623
72.8	4.933
86	5.466
103.8	5.981
125.2	6.514
142.8	6.944
165.2	7.477

TEST I.D. C1/9-2083/.5/22

PRINC. STRESS DIFFERENCE 2950 PSI (20.3 MPA)

TIME (HRS)	E1 (%)
0	0
35.778	.698
105.778	.99
253.556	1.241
412.222	1.406
449.556	1.534
497.778	1.605
595.778	1.718
737.333	1.845
841.556	1.95
942.667	2.051
1078	2.19
1222.67	2.34

TEST I.D. C2/9-2083/.5/22

PRINC. STRESS DIFFERENCE 4500 PSI (31.0 MPA)

TIME (HRS)	E1 (%)
0	0
5.778	1.242
24.444	2.813
56	3.938
103.111	5.578
150.222	6.68
210.667	7.875
257.333	9.07
294.667	10.43
331.556	11.766
356.444	13.242

TEST I.D. C1/9-2078.5/3.0/22

PRINC. STRESS DIFFERENCE 1700 PSI (11.7 MPA)

TIME (HRS)	E1 (%)
0	0
5.689	.07
20.978	.079
24.889	.085
190.933	.11
206.933	.116
226.133	.118
252.089	.118
280.889	.122
301.511	.123
310.756	.125

TEST I.D. C2/9-2078.5/3.0/22

PRINC. STRESS DIFFERENCE 4100 PSI (28.3 MPA)

TIME (HRS)	E1 (%)
0	0
12.8	1.269
31	1.831
53.4	2.294
83.2	2.738
102.8	2.969
127.2	3.244
146	3.45
161.8	3.613

TEST I.D. C1/9-2083.5/3.0/22

PRINC. STRESS DIFFERENCE 2900 PSI (20.0 MPA)

TIME (HRS)	E1 (%)
0	0
60	.85
146.667	1.04
238.667	1.217
364	1.385
494.667	1.509
624	1.644
766.667	1.746
914.667	1.88
1085.33	2.008

TEST I.D. C2/9-2083.5/3.0/22

PRINC. STRESS DIFFERENCE 4400 PSI (30.3 MPA)

TIME (HRS)	E1 (%)
0	0
26.444	2.306
88.667	4.031
180.444	5.344
309.556	6.544
466.667	7.688
653.333	8.756
857.111	9.694
1067.11	10.669
1247.56	11.325

TEST I.D. C3/9-2003.5/3.0/22

PRINC. STRESS DIFFERENCE 3000 PSI (20.7 MPA)

TIME (HRS)	E1 (%)
0	0
6.044	-.003
83.867	.003
155.644	.007
219.111	.012
292.4	.016
364.178	.021
425.378	.025
510	.029
563.644	.032
584.8	.036
673.956	.042

TEST I.D. C1/9-2625/.5/22

PRINC. STRESS DIFFERENCE 1200 PSI (8.3 MPA)

TIME (HRS)	E1 (%)
0	0
102.222	.131
360	.165
522.222	.168
788.889	.179
953.333	.184
1140	.197
1328.89	.199
1433.33	.208
1648.89	.213
1837.78	.217

TEST I.D. C2/9-2625/.5/22

PRINC. STRESS DIFFERENCE 2200 PSI (15.2 MPA)

TIME (HRS)	E1 (%)
0	0
16	.424
83.556	.716
176	.99
300.444	1.193
451.556	1.41
675.556	1.635
906.667	1.834
1153.78	2.033
1438.22	2.246

8

TEST I.D. C3/9-2625/.5/22

PRINC. STRESS DIFFERENCE 3300 PSI (22.8 MPA)

TIME (HRS)	E1 (%)
0	0
10	1.033
31.6	1.654
68.8	2.363
107.2	2.888
156.8	3.351
200	3.789
255.2	4.288
308.4	4.673
355.2	5.023

TEST I.D. C4/9-2625/.5/22

PRINC. STRESS DIFFERENCE 2300 PSI (16.1 MPA)

TIME (HRS)	E1 (%)
0	0
22.044	.04
71.111	.054
137.956	.075
209.067	.089
303.644	.103
393.244	.114
469.333	.119
504.178	.12
544	.131
593.778	.131

TEST I.D. C1/9-2677/3.0/22

PRINC. STRESS DIFFERENCE 1150 PSI (8.0 MPA)

TIME (HRS)	E1 (%)
0	0
29.467	.093
102	.115
195.689	.131
282.578	.135
385.333	.141
500.178	.148
639.956	.152
670.933	.153

TEST I.D. C1/9-2672.5/.03/100

PRINC. STRESS DIFFERENCE 1050 PSI (7.3 MPA)

TIME (HRS)	E1 (%)
0	0
19.2	.205
63.289	.505
146.489	.99
215.467	1.37
310.044	1.84
398.933	2.23
486.4	2.62
603.733	3.17

TEST I.D. C1/9-2624/.5/100

PRINC. STRESS DIFFERENCE 1000 PSI (6.9 MPA)

TIME (HRS)	E1 (%)
0	0
18.889	.319
44.578	.512
78.578	.731
127.689	1.041
200.978	1.348
327.156	1.772
399.689	2.03
494.133	2.314
578	2.581
652.8	2.783

TEST I.D. C1/9-2686/.5/100

PRINC. STRESS DIFFERENCE 1000 PSI (6.9 MPA)

TIME (HRS)	E1 (%)
0	0
53.2	.11
120.756	.196
200.133	.286
297.244	.398
413.778	.505
529.467	.618
636.711	.731
737.2	.823

TEST I.D. C2/9-2686/.5/100

PRINC. STRESS DIFFERENCE 2350 PSI (16.4 MPA)

TIME (HRS)	E1 (%)
0	0
30.8	2.75
64.4	4.781
95.822	6.281
125.067	7.313
154.933	8.75
184.489	10.406
218.4	12.906
247.333	16.063
260.4	17.625

TEST I.D. C1/9-2671/3.0/100

PRINC. STRESS DIFFERENCE 930 PSI (6.4 MPA)

TIME (HRS)	E1 (%)
0	0
69.333	.116
268	.308
417.333	.413
556	.52
785.333	.7
902.667	.798
1065.33	.909
1172	.978

TEST I.D. C2/9-2671/3.0/100

PRINC. STRESS DIFFERENCE 2250 PSI (15.9 MPA)

TIME (HRS)	E1 (%)
0	0
23.467	2
69.422	3.55
127.111	5.15
317.778	9.5
407.733	10.75
536.8	13.35
677.6	18.15
773.422	23.1
866.311	29.1

TEST I.D. C/9-2688/.5/200

PRINC. STRESS DIFFERENCE 1000 PSI (6.9 MPA)

TIME (HRS)	E1 (%)
0	0
9.147	1.785
22.12	2.731
29.587	3.443
40.413	4.176
52.08	4.856
64.773	5.61
79.8	6.449

TEST I.D. C1/9-2668/3.0/200

PRINC. STRESS DIFFERENCE 1000 PSI (6.9 MPA)

TIME (HRS)	E1 (%)
0	0
13.2	2.675
36.8	5.25
59.8	7.525
83.4	9.525
118	12.05
141.2	14.175
164.8	16.05

TEST I.D. C/7-2777/.5/22

PRINC STRESS DIFFERENCE 4800 PSI (33.1 MPA)

TIME (HRS)	E1 (%)
0	0
9.667	6.281
20.222	7.25
29.778	8.5
39.111	9.281
48.667	9.813
55.444	12.063
63.222	13.094
70.444	13.625
80	15.469
89.333	16.531
99.222	17.688

[illegible]

[illegible]

[illegible]

[illegible]

[illegible] Waste Management
[illegible] Management Division
[illegible]

[illegible]
Laboratory
[illegible]

[illegible]
[illegible] W. [illegible] Bennett
[illegible]

Oak Ridge National Laboratory
Box X
Oak Ridge, [illegible]
ATTN: [illegible] Blanko
[illegible] L. Claiborne
[illegible] Dole
[illegible] W. Huff
[illegible] E. Jenks

Battelle Pacific Northwest Labs
Battelle Blvd.
Richland, WA 99352
ATTN: [illegible] Bradley
[illegible] H. Jarrett
C. [illegible] Palmer
[illegible] Rupp
[illegible] Serne

Argonne National Laboratory
9700 S. Cass Avenue
Argonne, IL 60439
  ATTN: S. Fried
        A. M. Friedman
        L. Jardine
        M. Steindler

Westinghouse Electric Corp.
Waste Isolation Pilot Plant Project
Advanced Energy Systems Division
P.O. Box 40039
Albuquerque, NM 87016
  ATTN: Vincent F. Likar

Science Applications
1250 Prospect Street
La Jolla, CA 92037
  ATTN: David Bernstein

Science Applications
8201 Capwell Drive
Oakland, CA 94621
  ATTN: Ronald Hofmann

Union Carbide Corporation
Office of Waste Isolation
P.O. Box Y, Bldg. 9102-2
Oak Ridge, TN 37830
  ATTN: Dr. W. C. McClain

RE/SPEC, Inc.
P.O. Box 725
Rapid City, SD 57701
  ATTN: Dr. Paul Gnirk

University of California
Los Alamos Scientific Laboratory
Los Alamos, NM 87545
  ATTN: R. Brownlee   MS 570
        F. Riecker   MS 978
        W. J. Carter   MS 329

Lawrence Livermore Laboratory
P.O. Box 808
Livermore, CA 94550
  ATTN: R. N. Schock   L-437
        A. E. Lewis   L-207
        M. Hansen   L-200
        H. Heard   L-437

Center for Tectonophysics
Texas A&M University
College Station, TX
  ATTN: Dr. John Handin
        Director

Department of Earth Sciences
Dartmouth College
Hanover, NH
ATTN: Dr. John Lyons

Department of Civil Engineering'
Princeton University
Princeton, NJ
ATTN: Dr. George Pinder

University of Minnesota
Department of Civil & Mineral Engineering
112 Mines and Metallurgy Building
Minneapolis, MN 55455
ATTN: Dr. Charles Fairhurst

Center for Tectonophysics
Texas A&M University
College Station, TX
ATTN: Dr. J. E. Russell

University of California
Berkeley, CA 94720
ATTN: Dr. N. G. W. Cook

Department of Earth & Planetary Sciences
Massachussetts Institute of Technology
Cambridge, MA 02139
ATTN: Dr. W. F. Brace

State of New Mexico Environmental
Evaluation Group
320 Marcy Street, P.O. Box 968
Santa Fe, NM 87503
ATTN: Robert H. Neill, Director

U. S. Department of Energy, Headquarters
Office of Nuclear Waste Management
Washington, DC 20545
ATTN: Eugene F. Beckett, Proj. Cor. (WIPP) (5)
Colin A. Heath, Director (2)
Sheldon Meyers
Raymond G. Romatowski
R. Stein
Carl R. Cooley

U. S. Department of Energy, Albuquerque Opr.
P.O. Box 5400
Albuquerque, NM 87185
ATTN: D. T. Schueler, Manager (WIPP) (3)
R. Rudolph, Acting Depty Mgr.
G. Dennis, Director
S. C. Taylor (5)

U. S. Department of Energy
Carlsbad WIPP Project Office
Room 113, Federal Building
Carlsbad, NM 88220

Bechtel Inc.
P.O. Box 3965
San Francisco, CA 94119
ATTN: P. A. Langley
H. G. Taylor
P. K. Frobenius
D. L. Roberts
D. Duncan
J. Birkmyer

National Academy of Sciences
Committee on Radioactive Waste Management
2101 Constitution Avenue
Washington, DC 20418
ATTN: J. Holloway

Environmental Protection Agency
Ad-Hoc Panel of Earth Scientists
Department of Geological Sciences
Brown University
Providence, Rhode Island
ATTN: Dr. Bruno Giletti, Co-Chairman

Department of Geological Sciences
Harvard University
Cambridge, Massachusetts
ATTN: Dr. Raymond Siever, Co-Chairman

New Mexico Advisory Committee on WIPP
NMIMT Graduate Office
Socorro, NM 87801
ATTN: Marvin H. Wilkening, Chairman

DISTRIBUTION:

4000 A. Narath
4500 E. H. Beckner
4510 W. D. Weart
4511 L. R. Hill
4512 T. O. Hunter (10)
4512 A. R. Sattler
4512 J. R. Wayland (15)
4530 R. W. Lynch
4536 D. R. Andersen
4537 L. D. Tyler
4538 R. C. Lincoln
4540 M. L. Kramm
4541 L. W. Scully
4541 H. C. Shefelbine
4541 W. E. Wowak
4542 J. W. McKiernan
4542 Sandia WIPP Central Files (2) (T/C)
4700 J. Scott
4730 H. Stoller
4731 R. K. Traeger
4732 D. A. Northrop
4733 D. E. Munson
4734 A. L. Stevens
4736 A. F. Veneruso
5500 O. E. Jones
5521 S. W. Key
5521 R. D. Krieg
5521 C. M. Stone
5530 W. Herrmann
5531 L. D. Bertholf
5531 J. R. Tillerson
5531 P. R. Dawson
5532 B. M. Butcher (25)
5532 W. R. Wawersik (40)
8266 Tech. Library (2)
3141 Tech. Library (5)
3151 Tech. Writing (3)
For: DOE/TIC (Unlimited Release)
DOE/TIC (25)
(R. P. Campbell, 3172-3)
ALO S. Taylor, C&TI Div. (2)